Numerical simulation of leeside vortex: Case study

Jing-Shan Hong

Meteorological Information Center, Central Weather Bureau

Abstract

A pronounced lee-side vortex was observed over east of Taiwan during the Green Island Mesoscale Experiment (GIMEX). A high-resolution model simulation was performed in the paper to document the characteristics of the structure and evolution of the lee-side vortex.

During the initial stage of the lee-vortex, the model results show that the apparent downslope wind produces the subsidence warming over the south end of Central Mountain Range and then generate a lee-side mesolow near the coast of Taitung. Trajectory calculations suggest the lee-side subsidence is not only originated from the forced uplift upstream at surface layer but also from the downward motion at higher level. Qualitatively the air downward from the higher level (~4 km) is very similar to the supercritical hydraulic flow.

In addition to the formation of the mesolows formed at the lee side, a meso vortex is found and well coupled with the mesolow. The vorticity budget calculation show that, kinematically, the stretching effect is the most important vorticity generation term, which is due to the convergence as the inflow converged to the center of mesolows, and the corner-effect-enhanced curvature flow from Hengchun Peninsula encounters the strong dowslope wind. The leeside downward motion associated with the hydraulic-jump-flow also plays important role on initiating the lee-vortex in dynamically creating the low level potential vorticity.

1. Introduction

During the Mei-Yu season (May to June), mesolows at lower troposphere often form to the southwest, northwest and southeast of Taiwan (Kuo and Chen 1990; Chen 1992). In particular as a Mei-yu front is approaching and the prevailing pre-frontal southwestly flow impinges upon the Central Mountain Range (CMR), mesoscale low pressure centers usually form on the lee side of the mountain. Mesolows over Taiwan area usually have a horizontal scale about 150–200 km, a vertical extent from the surface to about 1500 m, an average life span of 12-15 h, and a sea level pressure perturbation of 3–5 hPa. The mesolows had a longer life span and stronger on the east side than the west side of the CMR. (Chen 1992). The mesolows were closely related to the rainfall distribution for those over northwestern Taiwan due to enhancing the southwesterlies (Chen and Chi 1980) and over southwestern Taiwan due to the enhanced low level convergence (Chen 1990). For those mesolows formed over southeast of Taiwan, subsidence warming due to the air originally at a higher level and latent heat release during the forced uplift along the windward slope are the possible mechanisms and suggested to indicate the warm, dry, and less rainfall in the low area (Kuo and Chen 1990; Chen 1992; Wang and Chen 2002).

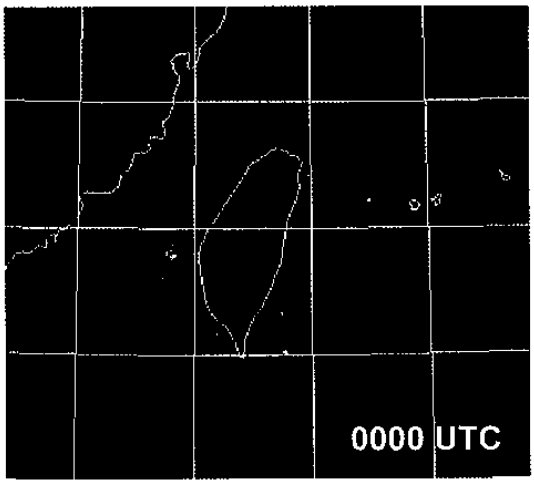

Fig. 1: The GMS visible images at 0000 UTC 7 May 2001..

Here this paper is to investigate a lee-side vortex case (as shown in Fig. 1) over the southeastern part of Taiwan during the Green Island Mesoscale Experiment (GIMEX) in 7 May 2001. Due to the lack of the observations over open ocean, it is difficult to identify the structure and evolution of the vortex case. The purpose of the paper, therefore, is to document the structure and evolution of this vortex case through the high-resolution model simulation to supplement the shortcoming from the deficiency of the observations. Section 2 is the description of the model configuration and the simulation results are given in section 3. Finally, the main conclusions are summarized.

2. Model description

The MM5 version 3.6 was initiated at 0000 UTC 6 May 2001 at the Central Weather

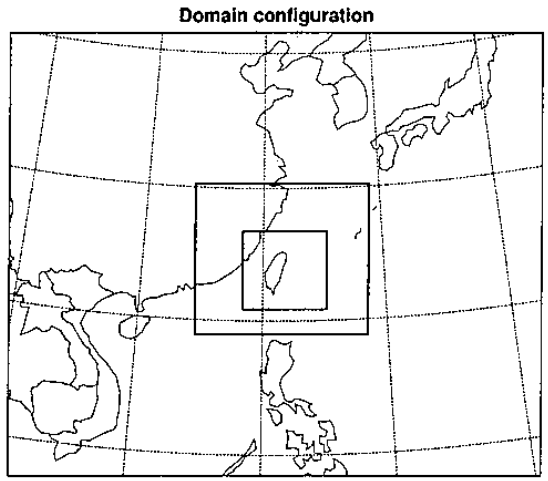

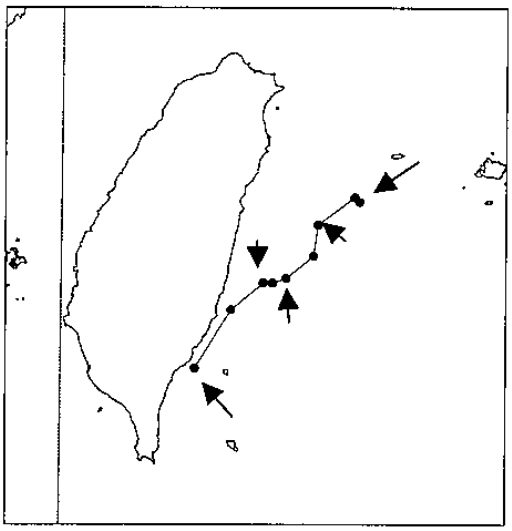

Bureau (CWB) of Taiwan. There were three nested domains, as shown in Fig. 2, with horizontal resolutions. (dimension) of 36-km (101x121), 12-km (103x118), and 4-km (160x172), respectively. The 34 unevenly spaced sigma levels were used in the vertical, with the maximum resolution in the boundary layer. The present study appears the configuration of the model domain to achieve the objective that the cloud-resolving resolution of 4-km domain covers all the evolution of the upstream environment and the lee vortex. All the MM5 simulations used the explicit Schultz microphysics scheme including ice and graupel/hail process, and the planetary boundary layer parameterization of NCEP's Medium Range Forecast scheme. A new version of Kain-Fritsch cumulus parameterization scheme includes shallow convection was applied in the 36- and 12-km domains, while no cumulus scheme was used in 4-km domain where convective processes could be resolved explicitly.

The initial atmospheric conditions and the sea surface temperature were obtained from the operational data assimilation system at CWB by using the optimal interpolation scheme at 45-km resolution and then interpolated to all the MM5 domains. Boundary conditions were forced from the forecasts of the operational global model at CWB with update interval of 6-hour. The 48-h forecast for all the MM5 domains was performed.

3. Numerical results

Fig. 3 is the track of model vortex derived from the vorticity centers with closed circulation at lowest half-sigma level (about 36 m AGL) of 4-km resolution. The figure showed that the lee-side vortex was initiated at 0600 UTC 6 May (6-hr forecasts) and very close to Taitung. The vortex moved northward along the coastline, tended to be stationary during 1200 ~ 1800 UTC 6 May, moved northeastward, and then dissipate at 0500 UTC 7 May. The life span for the model vortex is about 23 hours which is comparable with the observations in the literature (Chen 1992). In overall, the motion of the model vortex exhibited in a reasonable way and behaved similar as the observations except closer to the coastline.

Description and discussion for the four stages of the model vortex was inferred from the strength of the low pressure and the horizontal scale of the circulation; including initial stage (valid at 0600 ~ 1000 UTC 6 May), development stage (1100 UTC ~ 1800 UTC 6 May), mature stage (1900 UTC 6 May ~ 0000 UTC 7 May), and dissipate stage (0100 UTC ~ 0500 UTC 7 May). For the convenience, the term of the "vortex" in the following is substituted the usage of the "model vortex".

a. Initiation of the meso-low/lee-side vortex

The initial stage represented by the 8-hr model forecasts valid at 0800 UTC (1400 LST) 6 May is shown in Fig. 4. The figure showed that the upstream over southwest of Taiwan was dominated by the weak southwest flow. The apparent downslope wind produced the subsidence warming over the south end of CMR and then resulted in a lee-side mesolow along the coast of Taitung. Quantitatively estimate derived from the trajectory calculations as shown in Fig. 5 suggested the lee-side subsidence was not only originated from the forced uplift upstream at surface layer (trajectory 2) but also from the downward motion at higher level (trajectory 1). Table 1 lists the diagnostics following the trajectories and shows that the difference of the altitude of the location for the trajectory 2 at 4-hr

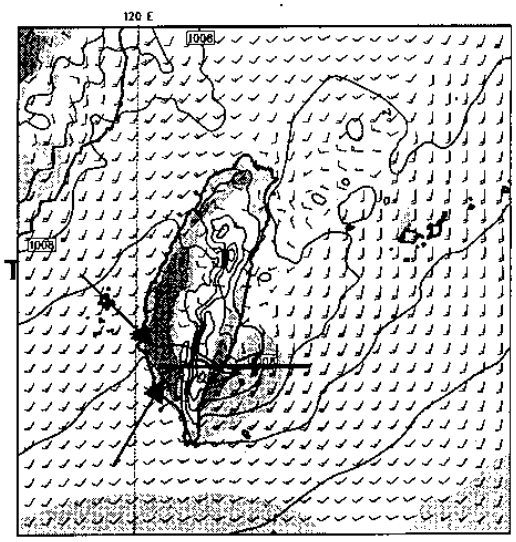

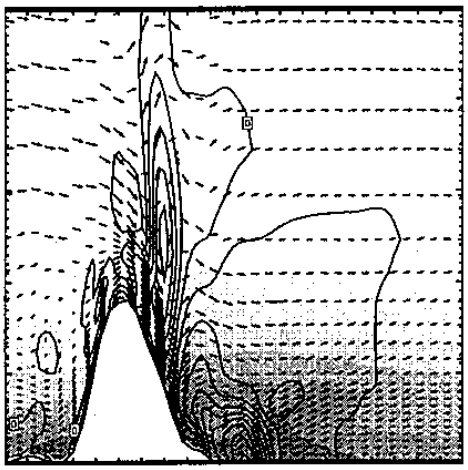

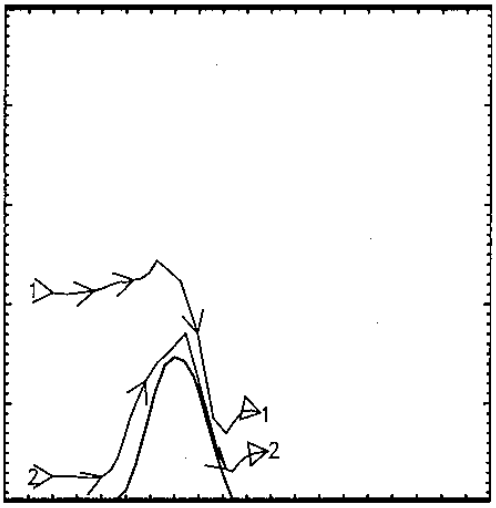

Fig. 5: The trajectory 1, and 2 projected to the cross section as shown in Fig. 4a.

deepened and decelerated upon crossing the jump, and a low formed downstream of the jump. Therefore, the subsidence warming due to the latent heating during the forced uplift on the windward surface layer and the adiabatic heating from the nonlinear hydraulic-jump-like flow are suggested to be important mechanisms for the formation of the lee-side mesolow.

Table 1: The diagnostics follow the trajectory 1 and 2 for the altitude of the location (H, m), absolute vorticity ($f+\zeta$, 10^{-5} s^{-1}), potential vorticity (PV, PVU), potential temperature (θ, K), and temperature (T, °C).

Trajectory 1

Forecast time	H	$f+\zeta$	PV	θ	T
4	2117	4.73	0.21	308.10	15.13
5	2140	4.80	0.11	307.96	14.73
6	2250	8.88	0.33	306.92	12.64
7	1717	41.63	3.99	308.85	19.48
8	910	82.93	1.77	306.97	25.56

Trajectory 2

Forecast time	H	$f+\zeta$	PV	θ	T
4	267	10.91	.24	301.07	26.25
5	266	19.48	-.07	303.28	28.38
6	1231	3.59	.46	303.34	19.07
7	341	124.61	.42	306.71	30.78
8	523	73.00	2.36	305.95	28.30

and 7-hr forecast were 74 m, however, the potential temperature and temperature were increased about 5.6 K and 4.5 °C. The increased potential temperature was mainly due to the diabatic latent heating during the parcel forced uplift at the windward side. On the other hand, trajectory 1 was forced downward and almost following adiabatic warming from 15.13 to 25.56 °C as the parcel descended from 2117 m to 910 m. The strong downward motion occurred over the mountain and lee side between 1~4 km AGL as shown in Fig. 4b is qualitatively very similar to the supercritical hydraulic flow (Epifanio and Durran 2002a, b) characterized as the accelerated upstream of the jump, the flow

A closed circulation for the meso vortex was first detected in the model at 0600 UTC 6 May. To better understand the formation mechanism of the meso vortex, a budget calculation formulated from the vorticity equation in σ coordinate was performed to evaluate the various terms as follows:

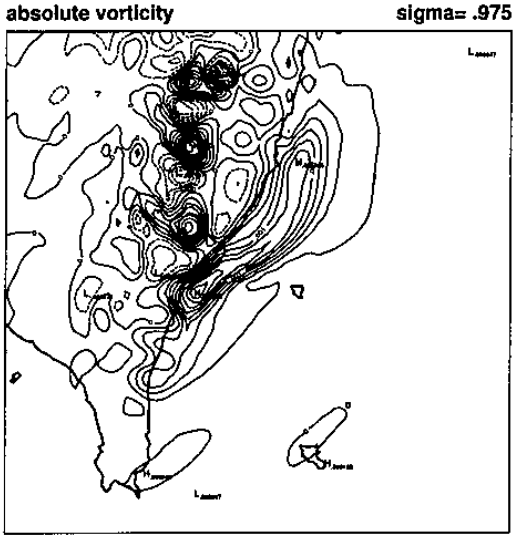

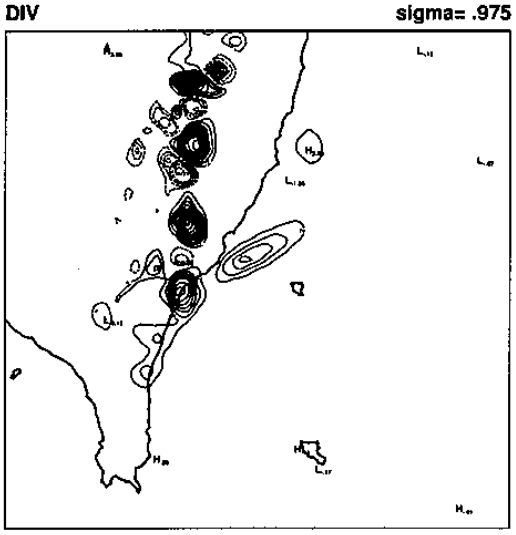

$$\frac{\partial(f+\zeta)}{\partial t} = -\vec{V}\cdot\nabla(f+\zeta) - \dot{\sigma}\frac{\partial\zeta}{\partial\sigma} - (f+\zeta)\nabla\cdot\vec{V} -$$

TOTAL HADV VADV DIV

$$\left(\frac{\partial\dot{\sigma}}{\partial x}\frac{\partial v}{\partial\sigma} - \frac{\partial\dot{\sigma}}{\partial y}\frac{\partial u}{\partial\sigma}\right) - \frac{R}{P_s}\left(\frac{\partial T}{\partial x}\frac{\partial P_s}{\partial y} - \frac{\partial T}{\partial y}\frac{\partial P_s}{\partial x}\right)$$

TILT SOL

On the right hand side of the equation, HADV and VADV are the horizontal and vertical advection term, respectively. DIV denotes the stretching effect due to the divergence. TILT is the tilting term and SOL is the solenoidal term. All the terms on the right hand side can be calculated at each grid; consequently, a summation of these terms represented the estimated local change of vorticity (TOTAL).

Fig. 6 is the calculated results of DIV term at σ =0.975 while the other terms are too small and are neglectable. Fig. 6a showed that the vorticity pattern over land area was rather complicate due to the boundary layer and precipitation process. Here the study is in particular focused on the elongate offshore vorticity maximum extended from the center of the mesolow at foothill toward the northeast. The vorticity maximum provided a rotational background and was mainly due to the horizontal shear associated with the strong southwest curvature flow (Fig. 4a). The budget calculations showed that the estimated vorticity generation term for the offshore vorticity maximum was mainly contributed from the DIV term and partially offset by the HADV and TILT terms (not shown). It is noted that the DIV term exhibited two maximums; the south one was located close to Taitung, and the second took an elongated shape at northeast of Taitung. Kinematically, the DIV was associated with the low level convergence due to the inflow converged to the center of the mesolow, and the corner-effect-induced southwestlies encountered the strong dowslope wind along the coastline as shown in Fig. 4a. Furthermore, the stretching effect was enhanced by the convergence which was embedded in a shear background.

On the other hand, as mentioned, The strong downward motion occurred over the mountain and lee side between 1~4 km AGL is qualitatively very similar to the supercritical hydraulic flow. Epifanio and Durran (2002b) point out that the potential vorticity generation is found to result mainly from thermal dissipation and tends to diabatically modify the potential temperature field in the jump. Table 1 showed that the potential vorticity following the trajectory 1 had an abrupt increase at 7-hr and 8-hr forecast and then resulted in the increase of the absolute vorticity. Therefore, the leeside downward motion plays important roles on initiating the lee-vortex in kinematically stretching the vorticity as converged with the corner-effect-induced curvature flow, and in dynamically creating the potential vorticity from the hydraulic-jump-like flow at higher level.

b. Development stage

Fig. 7 is the 15-hr model forecast valid at 1600 UTC 6 May and represent the development stage of the lee vortex. The figure showed that there existed stagnation point associated with the pressure ridge at the upstream and split the impinged inflow to the north and south. The north branch contributed to the so-called "offshore convergence" (Yeh and Chen 2002) occurred along the northwestern coast of Taiwan. Similar to the initial stage, the south branch coupled with the corner effect resulted in the strong southwest flow. The lee-side vortex coupled with the

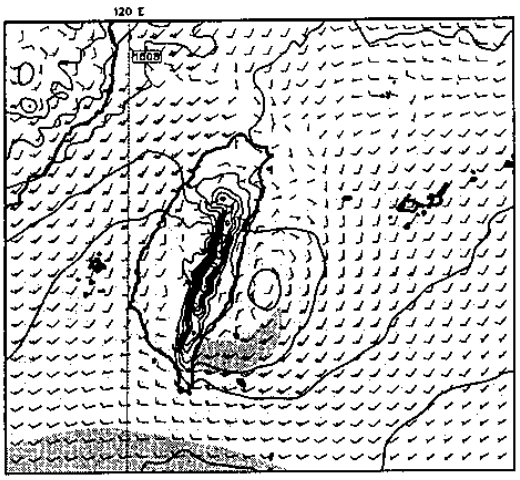

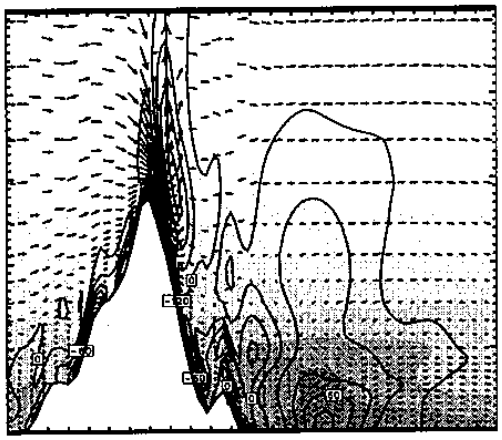

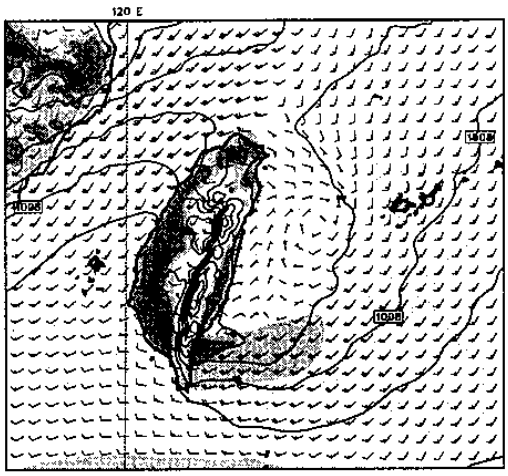

Fig. 11: Same as Fig. 4 but for 28-hr forecast (valid at 0400 UTC, 7 May).

mesolow has been moved downstream away from its origin location. The vortex had the elongated structure with the size of about 200×140 km. The elongate structure was the result of the combination of the lee vortex itself coupled with the stretching just south end of the vortex, which was due to the convergence as the corner-effect-enhanced southwest flow met the southward flow associated with the vortex. The cross section across the vortex center as shown in Fig. 7b showed that the vortex possessed warm/dry air and had the upright vertical extension up to 3 km AGL but the most pronounced circulation was below 1 km AGL.

c. mature and dissipate stage

Fig. 8 is the mature stage of the lee-side vortex with the larger circulation coverage (~220×220 km^2) but weaker than the development stage (Fig. 7). The figure showed that the vortex become more axis symmetry and upscale development. It is suggested the vortex went through the axisymmetrization process (Smith and Montgomery 1995) from the asymmetric wavenumber 2 to wavenumber 1 structure. It is noted that the wavenumber 2 structure of the vortex was not the vortex Rossby wave as observed in the typhoon's inner core structure but externally forced by the topography as depicted in the previous sub-section. Because of the absence of the vorticity generation and the convection in the warm/dry core of the vortex, the vortex is expected to evolve through its internal dynamics via the simply geostrophic adjustment thinking during the period. Due to the scale of the vortex is quite small (typically O (100 km)), thus the adjustment is approximately the same as in a non-rotating system and the low pressure will be suppressed by to the low level convergence. One another important factor to affect the vortex structure is the vertical wind shear. The vertical wind shear result in the vortex tilts to the downshear side (not shown here), which would hurt the maintenance of the vortex.

4. Concluding remarks

The Green Island Mesoscale Experiment (GIMEX) over southeast Taiwan was conducted in the Mei-Yu season of May and June during 2001. During the experimental period, a pronounced lee-side vortex was observed from the GMS visible images over southeast of Taiwan in 7 May 2001. The purpose of the study is to document the characteristics of the structure and evolution of this case through the high-resolution simulation by using the PSU – NCAR MM5 model.

The model vortex at 4-km resolution, with life span about 23 hours, was initiated at 0600 UTC 6 May (6-hr forecasts) near the coast of Taitung and moved slowly to the northeast. In overall, the motion of the model vortex exhibited in a reasonable way and behaved similar as the observations except closer to the coastline. Four

life stages in the simulation were defined to further discuss the detail structure and evolution of the model vortex.

Trajectory calculations suggested the lee-side subsidence was not only originated from the forced uplift upstream at surface layer but also from the downward motion at higher level. Qualitatively the air downward from the higher level (~4 km) were very similar to the supercritical hydraulic flow (Epifanio and Durran 2002a, b) characterized as the accelerated upstream of the jump, the flow deepened and decelerated upon crossing the jump, and a low formed downstream of the jump. Therefore, the subsidence warming due to the latent heating during the forced uplift on the windward surface layer and the adiabatic heating from the nonlinear hydraulic-jump-like flow are suggested to the important mechanisms for the formation of the lee-side mesolow.

In addition to the formation of the mesolow formed at the lee side, a meso vortex was found and well coupled with the mesolow. The vorticity budget calculation showed that, kinematically, the stretching effect was the most important vorticity generation term, which was due to the convergence as the inflow converged to the center of mesolows, and the corner-effect-enhanced southwestlies encountered the strong dowslope wind. On the other hand, the leeside downward motion associated with the hydraulic-jump-flow also plays important role on initiating the lee-vortex in dynamically creating the low level potential vorticity.

During the development stage, the lee-side vortex coupled with the mesolow was moved downstream away from its origin location and exhibited as an elongate structure. The vortex had the upright vertical extension up to 3 km AGL but the most pronounced circulation was below 1 km AGL. The elongate structure was the result of the combination of the lee vortex itself coupled with the stretching just south end of the vortex, which was due to the convergence as the corner-effect-enhanced southwest flow met the southward flow associated with the vortex.

The further analysis also point out there were three factors play important roles in controlling the following evolution of the lee-vortex. First, during the mature stage of the lee-side vortex, the vortex went through the axisymmetrization process from the asymmetric wavenumber 2 to wavenumber 1 structure. Second, due to the small scale of the vortex, the geostrophic adjustment process will fill up and suppress the vortex. Third, the vertical wind shear tilts the vortex to the downshear side, which would further destroy the vertical structure of the vortex.

Acknowledgments

The author extends his sincere gratitude to the Meteorological Information Center at the Central Weather Bureau of Taiwan for offering the utmost support. The computations were performed on the Fujitsu VPP5000 computer with 4 processor elements. The author also thanks all participants, in particular Prof. B. J.-D. Jou, involved in the planning and field phase of GIMEX. This research was supported by the National Science Council of Taiwan under Grant NSC 91-2111-M-052-002 and NSC 91-2119-M-002-032.

Reference:

Chen, G. T. J., 1990: Study of rainfalls and radar echoes in the heavy rainfall events accompanied by mesolow in Mei-Yu season. *Atmos. Sci.*, **18**, 213 – 228. (In Chinese with English abstract).

Chen, G. T. J., 1992: Mesoscale features observed in Taiwan Mei-Yu season. *J. Meteor. Soc. Japan*, **70**, 497 – 516.

Chen, G. T. J., and S. S. Chi, 1980: On the frequency and speed of Mei-Yu front over southern China and the adjacent areas. *Paper Meteor. Res.*, **3, 1&2,** 31 – 42.

Epifanio, C. C., and D. R. Durran, 2002a: Lee-vortex formation in free-slip stratified flow over ridges. Part I: Comparison of weakly nonlinear inviscid theory and fully nonlinear viscous simulations. *J. Atmos. Sci.*, 1166–1181.

——, and ——, 2002b: Lee-vortex formation in free-slip stratified flow over ridges. Part II: Mechanisms of vorticity and PV production in nonlinear viscous wakes. *J. Atmos. Sci.*, 1166–1181.

Kuo, Y. H., and G. T. J. Chen, 1990: The Taiwan Area Mesoscale Experiment (TAMEX): An overview. *Bull. Amer. Meteor. Soc.*, **71**, 488 - 503.

Smith, G. B., and M. T. Montgomery, 1995: Vortex axisymmetrization and its dependence on azimuthal wavenumbers or asymmetric radial structure changes. *Quart. J. Roy. Meteor. Soc.*, **121**, 1615 – 1650.

Wang, C. C., and G. T. J. Chen, 2002: Case study of the leeside mesolow and mesocyclone in TAMEX. *Mon. Wea. Rev.*, **130**, 2572 – 2592.

Yeh, H. C., and Y. L. Chen, 2002: The role of offshore convergence on coastal rainfall during TAMEX IOP3. *Mon. Wea. Rev.*, **130**, 2709 – 2730.